ARCHITECTURE CIVIL ENGINEERING ENVIRONMENT
The Silesian University of Technology No. 3/2011

NUMERICAL ANALYSIS OF STRUCTURAL COMPONENTS IN POWER GENERATION FACILITIES

Stanisław PIETRUSZCZAK*

* Prof.; McMaster University, Hamilton, Ont., Canada
E-mail address: *pietrusz@mcmaster.ca*

Received: 15.07.2011; Revised: 15.08.2011; Accepted: 1.09.2011

Abstract

This paper addresses the issue of modeling of inelastic response of large–scale civil structures built of either masonry or heavily reinforced concrete. It consists of two parts that examine the mechanical characteristics of both these classes of materials and present applications of the respective mathematical frameworks to some real engineering structures. For masonry, a methodology is described for identification of macroscopic properties based on a meso-scale approach which employs a finite element analysis at the level of the Representative Elementary Volume. The procedure is illustrated by an example that involves the analysis of masonry components of a hydroelectric power generation facility in Quebec (Canada). For reinforced concrete, a non-linear continuum theory is reviewed that describes the mechanical effects of alkali-aggregate reaction (AAR) The formulation is applied to examine the mechanical behaviour of some reinforced concrete structures in nuclear power facilities located, once again, in Quebec (Canada).

Streszczenie

Poniższy artykuł dotyczy nieliniowego modelowania wielkogabarytowych konstrukcji inżynierskich wykonanych z cegły lub silnie zbrojonego betonu. Artykuł składa się z dwóch odrębnych części, które opisują własnosci mechaniczne obu materiałów i przedstawiają zastosowania do praktycznych problemów inżynierskich. Dla konstrukcji murowych przestawiona jest metodologia identyfikacji makroskopowych własnosci mechanicznych, która opiera sie na analizie numerycznej (w skali mezoskopowej) Elementarnej Objętości Reprezentatywnej. Procedura zilustrowana jest przykładem numerycznym dotyczącym analizy konstrukcji murowych w jednej z elektrowni wodnych w Quebec (Kanada). Dla konstrukcji żelbetowych przedyskutowane jest nieliniowe sformułowanie opisujące efekty mechaniczne reakcji alkalicznej w betonie. To podejście jest zastosowane do analizy elementów konstrukcyjnych w elektrowni atomowej zlokalizowanej również w Quebec (Kanada).

Keywords: **Brick masonry; Reinforced concrete; Homogenization; Chemo-plasticity.**

1. INTRODUCTION

The analysis of large civil structures made of composite materials, like brick masonry and/or heavily reinforced concrete, should best be conducted at a macro-scale. In this case, the material can be described as a continuum whose average properties are identified at the level of constituents taking into account their geometric arrangement.

For structural masonry, several different approximations have been developed for assessing the average properties. Those include the micropolar Cosserat continuum models (e.g. Sulem and Muhlhaus [1], Masiani and Trovalusci [2]) as well as the estimates based on the theory of homogenization for periodic media (e.g., Anthoine [3-4]). In addition, a significant work has also been undertaken with regards to the development of phenomenologicaly-based macroscopic failure criteria. Examples include the studies of Lourenço et al. [5], Raffard et al. [6] and Ushaksaraei and Pietruszczak [7].

For heavily reinforced concrete structures, such as hydraulic or nuclear ones, the presence of reinforcement cannot be modeled in a discrete way, as this would be beyond the capabilities of modern day computers. Thus, the material should also be considered as a composite medium comprising the concrete matrix and a set of families of reinforcement.

The overall macroscopic behaviour can then be defined by employing suitable averaging techniques. Several approaches of this type have been developed in the past; the examples include the works of Scordelis [8], Crisfield & Wills [9], Pietruszczak & Winnicki [10].

This paper consists of two main parts. The first part deals with the unreinforced masonry and is focused on presenting a methodology for deriving the equivalent continuum properties from a meso-scale approach. The approach is verified by simulating the experiments conducted by Page [11-12], which involve a series of biaxial load-controlled tests carried out at different orientations of the bed joints. The constituents have been modeled using a plasticity framework that accounts for the onset and propagation of localized deformation. The first approach examined here involves the finite element simulations of entire panels. Later, the formulation is simplified by solving the associated boundary-value problem over a suitably chosen Representative Elementary Volume subjected to periodic boundary conditions. The meso-scale approach described above has been employed to define the macroscopic properties of masonry components of some hydroelectric power generation facilities in Quebec, Canada. Those include masonry structures of the Pugan hydroelectric power station located on the Gatineau River in Quebec, Canada. Here, a series of dynamic analyses have been conducted that examine the impact of seismic retrofit of the masonry walls on their overall stability.

In part two of this paper, the issue of modeling of reinforced concrete structures affected by chemo-mechanical degradation is addressed. In particular, the focus is on nuclear power plant structures suffering from the effects of continuing alkali-aggregate reaction. The mechanical behaviour of reinforced concrete affected by AAR is described by employing a non-linear continuum theory that incorporates a chemo-mechanical coupling (Winnicki & Pietruszczak [13]). The governing constitutive relations, which have been incorporated in a finite element code, are first reviewed. Later, the results of numerical studies are presented. First, the mechanical response of a containment structure in a nuclear facility located near the community of Trois-Rivières in Québec is examined. The structure is subjected to continuing AAR followed by a seismic event typical for the region. Subsequently, an inelastic analysis is carried out for a spent fuel exchange room in the nuclear reactor building.

2. NUMERICAL ANALYSIS OF LARGE-SCALE MASONRY STRUCTURES

2.1. Assessment of macroscopic properties of masonry

A direct approach for specification of properties of structural masonry involves the experimental testing of masonry panels. One of the most comprehensive sets of experimental data for in-plane loading of masonry at various orientations of bed joint is that obtained by Page [11-12]. The tests were conducted under biaxial compression and biaxial tension-compression and were carried out on square half-scale panels. Apparently, the experimental testing is expensive, time-consuming and the scatter of the results is significant. A pragmatic alternative is the use of numerical/analytical tools to predict the response of structural masonry based on properties of constituents, which can be identified from standard material tests. Such an approach is more flexible in terms of specification of material parameters and will be pursued here.

The accuracy of the assessment of macroscopic properties depends strongly on the constitutive relation employed to describe the response of constituents. The specific form used here is that outlined in the article by Shieh-Beygi & Pietruszczak [14]. For the completeness of the presentation, the key assumptions embedded in this framework are reviewed below.

The behaviour of both constituents, i.e. bricks and mortar, is assumed to be elastic-brittle in tension regime, while for compressive stress trajectories, plastic-brittle characteristics are employed. Thus, in tension domain the yield and failure surfaces coincide with each other. However, in compression regime a distinct yield surface is introduced a priori, whose evolution is attributed to accumulated plastic distortions. Thus,

$$f_1 = \sigma_1 - \sigma_0 = 0; \qquad f_2 = \frac{\bar{\sigma}}{g(\theta)} + \eta(\xi)\sigma_m - \upsilon = 0 \qquad (1)$$

In Eq.(1), σ_m , $\bar{\sigma}$ and θ represent a set of invariant measures of the stress tensor (cf. Nayak & Zienkiewicz [15]), σ_0 is the tensile strength of the material and ξ is an internal variable whose evolution is a function of deviatoric plastic strain history, i.e. $\dot{\xi} \propto \dot{e}_{ij}^{p}\, \dot{e}_{ij}^{p}$. Moreover, $\eta(\xi)$ is a monotonically increasing variable and for $\xi \to \infty$ there is $\eta \to \eta_f$, where η_f refers to the conditions at failure.

Prior to the onset of localization, the loading/unloading criteria are established using the

classical Kuhn-Tucker conditions and the elastoplastic operator is obtained following the standard plasticity procedure, i.e. invoking consistency condition and the additivity postulate. This leads to

$$D_{ijkl} = D^e_{ijkl} - \frac{1}{H_e + H_p}\left(D^e_{ijpq}\frac{\partial \psi}{\partial \sigma_{pq}}\frac{\partial f_2}{\partial \sigma_{mn}} D^e_{mnkl} \right)$$

$$H_e = \frac{\partial f_2}{\partial \sigma_{ij}} D^e_{ijkl}\frac{\partial \psi}{\partial \sigma_{kl}}; \qquad (2)$$

$$H_p = -\frac{\partial f_2}{\partial \xi}\left(\frac{1}{2}\mathrm{dev}\frac{\partial \psi}{\partial \sigma_{ij}}\mathrm{dev}\frac{\partial \psi}{\partial \sigma_{ij}} \right)^{1/2}$$

in which D^e_{ijkl} represents the elastic constitutive operator, and ψ is the plastic potential.

The conditions at failure are said to be associated with formation of a macrocrack, whose direction is consistent with either Rankine's and Mohr-Coulomb representation, viz. Eq.(1). In the post-localized range, a simple volume averaging procedure is employed based on the work reported by Pietruszczak [16]. The procedure incorporates the stress/strain rate averaging and the deformation within the fractured zone is defined in terms of velocity discontinuities across the interface, $\dot{g}_i$. The averaged macroscopic constitutive relation is expressed as

$$\dot{\sigma}_{ij} = D_{ijpq}\left(\delta_{pk}\delta_{ql} - \mu\, n_p S_{qkl} \right)\dot{\varepsilon}_{kl} \qquad (3)$$

where

$$\dot{g}_i = S_{ijk}\dot{\varepsilon}_{jk};$$

$$S_{ijk} = E^{-1}_{ip} D_{pqjk} n_q;$$

$$E_{ij} = K_{ij} + \mu\, D_{ipqj} n_p n_q \qquad (4)$$

In equations above, μ is a characteristic dimension that is defined as the ratio of the surface area of the localization plane to the volume of the element. Furthermore, K_{ij} is the elastoplastic operator specifying the response within the localized zone. The latter is defined here by incorporating a strain-softening plasticity framework and the details of the specification of this operator are provided in the original reference [14].

2.1.1. Simulations of tests conducted by Page

In order to illustrate the methodology for specification of material characteristics of masonry, the experimental tests conducted by Page [11-12] are considered. The tested specimens consisted of square 360×360 mm panels with half-scale bricks. The samples were subjected to a series of biaxial load-controlled tests that were conducted at five different orientations of the bed joints θ, viz. 0°, 22.5°, 45°, 67.5°, and 90°. The results from all orientations were then collected to obtain a comprehensive picture of the directional strength characteristics of brick masonry.

The first approach examined here involves the finite element simulations of entire panels tested by Page (see Ref. [14]). The simulations were based on the

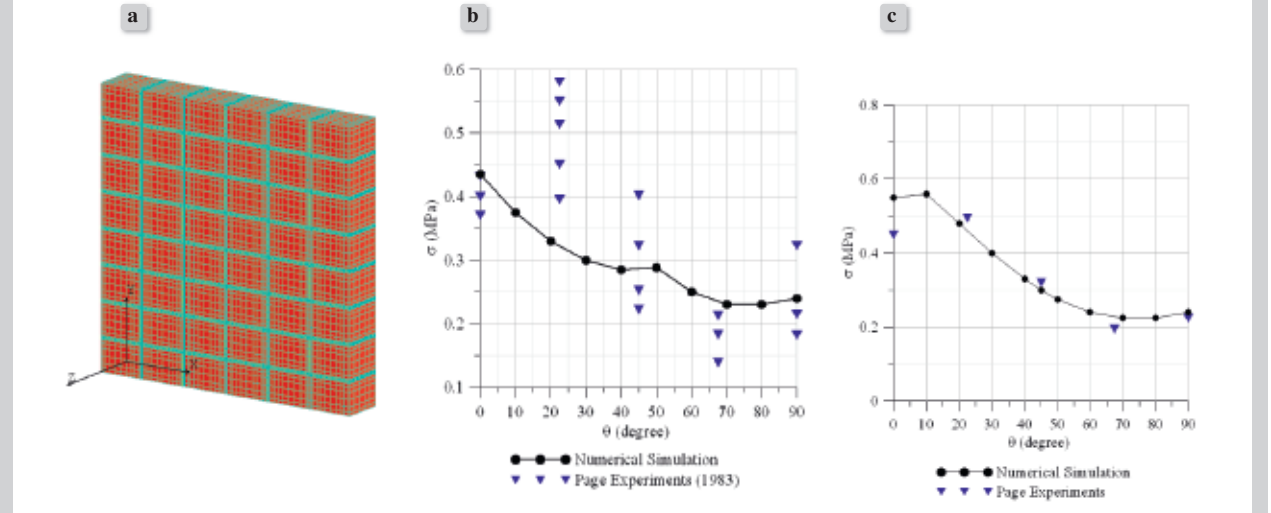

Figure 1.
Numerical simulations of panels tested by Page (1983); (a) FE discretization; (b) & (c) failure envelopes for uniaxial tension and biaxial compression-tension (σ_c/σ_t=1.0), respectively (after Shieh-Beygi & Pietruszczak [14])

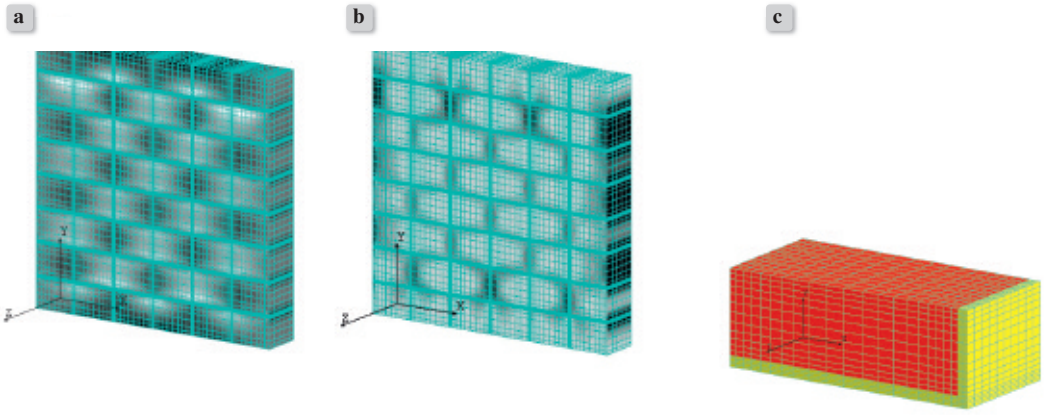

Figure 2.
The distribution pattern of (a) maximum principal stress; (b) minimum principal stress in biaxial tension-compression θ=10°; (c) REV and its finite element discretization (after Shieh-Beygi & Pietruszczak [14])

framework outlined in Section 2.1. The specimens were discretized using a three dimensional mesh with over 30,000 8-noded solid elements, Fig. 1a. The analysis was carried out for different orientations of the bed joints relative to the loading direction. For each orientation, two different loading patterns were considered, namely uniaxial tension and biaxial tension-compression with the ratio of vertical to horizontal traction $\sigma_c/\sigma_t = 1$ (equivalent to a pure shear at 45°). The basic material parameters, for both constituents, are provided in the original reference.

The key results are given in Figs. 1b and 1c, which present the directional strength characteristics. It is seen from Fig.1b that the experimental data is quite the numerical predictions, however, are in a fairly good agreement with the respective mean values. The failure modes corresponding to different configurations are quite diversified and the details, once again, are discussed in the original article.

An important aspect of the solution is the periodicity of stress/displacement field for any given orientation. As an example, Fig. 2 shows the distribution of the principal stresses for $\theta = 10°$. It is evident here that the stress field is periodic within the entire domain, except for the regions adjacent to the boundaries. The notion of periodicity can be exploited by introducing an approach based on numerical homogenization. Thus, rather than considering the entire panel, the boundary value problem can be solved over a suitably chosen Representative Elementary Volume (REV), subjected to periodic boundary conditions. As an illustration of this approach, the key results reported in Ref. [14] are provided here. The adopted REV was discretized

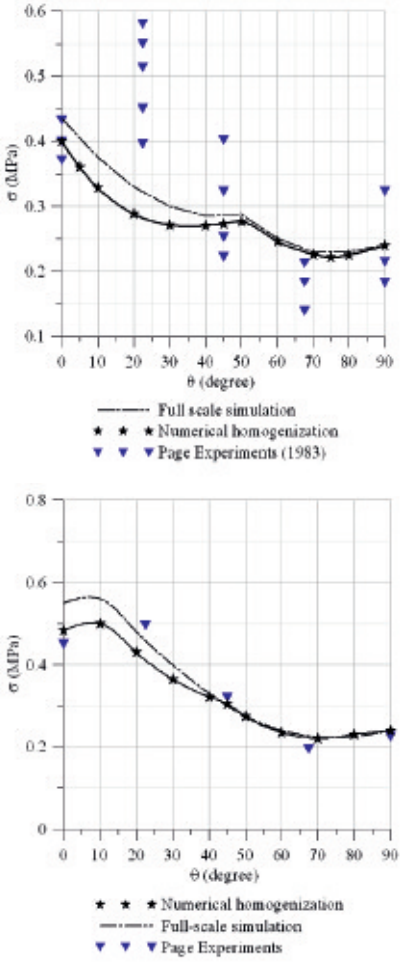

Figure 3.
Directional strength characteristic for uniaxial tension and biaxial compression-tension; comparison between the results for the full-scale and REV simulations (after Shieh-Beygi & Pietruszczak [14])

using approx. 3800 8-noded solid elements, Fig. 2c. Again, a load-controlled scheme was used in the analysis and the ultimate load was identified with the onset of global instability.

Fig. 3 shows the strength characteristics for different orientations of the bed joints. It can be seen that the results for RVE are close to those obtained from the full-scale tests. The difference stems mainly from the influence of boundary conditions that affect the local stress/strain fields. Apparently, the difference between the full-scale simulations and the REV will decrease by increasing the size of the test panels.

As mentioned earlier, the methodology outlined above can be employed to generate the data on the directional strength properties of masonry. This information can then be used for the purpose of identification of material functions that appear in a macroscopic formulation of the problem.

2.2. Macroscopic framework; critical plane approach

The mathematical framework used at the macroscopic level employs an elastic-brittle idealization. The argument here is that under a seismic excitation, which is of main interest in this work, the predominant failure mode is a tensile fracture, which is of a brittle nature. The onset of localization and the orientation of the failure plane are derived from the critical plane approach (Pietruszczak & Mroz [17]) by solving a constrained optimization problem. The response in the post-localized regime is modeled by employing the volume averaging procedure that incorporates representation (3) of Section 2.1.

The specific form of macroscopic failure criterion is that developed in Ref. [7]. It incorporates a linear Coulomb failure function with a cut-off in tension domain, which is analogous to representation (1)

$$F_1 = \sigma_n - \sigma_0; \qquad F_2 = \tau + \sigma_n \tan(\phi) - c \qquad (5)$$

used at the meso-level, i.e.

where $\tau = \sigma_{ij} n_i s_j$; $\sigma_n = \sigma_{ij} n_i n_j$ are the shear and normal components of the traction vector on the plane with unit normal n_i and s_i $n_i = 0$. In Eq.(5), the material parameters σ_0, ϕ and c are defined in terms

$$\begin{aligned}
\sigma_0 &= \sigma_{01}(1+\Omega_{ij}^{\sigma_0} n_i n_j) + \sigma_{02}(\Omega_{ij}^{\sigma_0} n_i n_j)^2 + \sigma_{03}(\Omega_{ij}^{\sigma_0} n_i n_j)^3 + \ldots\ldots \\
\phi &= \phi_1(1+\Omega_{ij}^{\phi} n_i n_j) + \phi_2(\Omega_{ij}^{\phi} n_i n_j)^2 + \phi_3(\Omega_{ij}^{\phi} n_i n_j)^3 + \ldots\ldots \qquad (6) \\
c &= c_1(1+\Omega_{ij}^{c} n_i n_j) + c_2(\Omega_{ij}^{c} n_i n_j)^2 + c_3(\Omega_{ij}^{c} n_i n_j)^3 + \ldots\ldots
\end{aligned}$$

of orientation-dependent functions

Here, the parameters $\sigma_{01}\ldots, \phi_1, \ldots c_1$ are the distribution coefficients and Ω's are symmetric traceless tensors which describe the bias in the spatial variation of the strength parameters. The orientation of the localization plane can be determined by maximizing the failure functions F_1 and F_2, Eq.(5), with respect to n_i and s_i, subject to constraints $n_i n_i = 1$; $s_i s_i = 1$; $n_i s_i = 0$. For the given orientation, the conditions at failure correspond to $\max\{F_1, F_2\} = 0$.

The identification of material parameters is based, in general, on the methodology analogous to that outlined in Section 2.1.1.

2.3. Numerical simulations of masonry walls of Paugan power station

The example provided here, which illustrates the proposed methodology, is related to the seismic analysis of masonry walls of Paugan power station located near Hull, Quebec (Pietruszczak & Gocevski [18]). The intake structure was built in 1927 and, over the last few decades, it has suffered a significant damage due to continuing alkali-aggregate reaction. Periodic repairs were made in 1947 (grout curtains and concrete repairs at various locations) and, more recently, in 1990 when slot cuts were made between the gravity section/ auxiliary spillway as well as the intermediate section and the intake. The powerhouse of the Paugan hydroelectric plant has non-bearing masonry walls that serve as enclosures. The primary interest of this study is the assessment of the stability of these walls under a seismic excitation typical for the region.

The assessment of strength properties of the Paugan brickwork involved the simulations of the response in uniaxial tension, pure shear and biaxial compression-tension ($\sigma_c/\sigma_t = 2.33$) for different orientations of the bed joints. For all these loading histories, the behaviour is primarily governed by the properties of the mortar joints. For the Paugan masonry, the key strength properties, i.e. tensile strength, cohesion and the friction angle, are $\sigma_0 = 0.18$ MPa, $c = 0.24$ MPa, $\phi = 45°$, respectively. The units of the brickwork have the dimensions of 208×98×61 mm, while the mortar joints are approx. 10 mm thick. In the identification process, the set of data corresponding to uniaxial tension, was employed for specification of the parameters embedded in the distribution of σ_0, eq.(6). The predicted strengths in pure shear and biaxial compression-tension were then used for specification of constants appearing in the distribution of ϕ and c. The details on the identification procedure, which employs

Figure 4.
The outside and inside views of the powerhouse

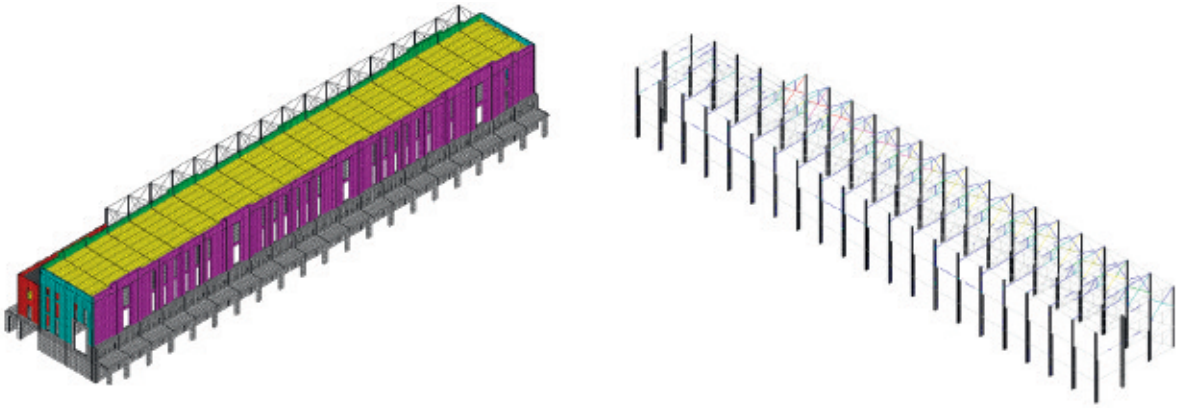

Figure 5.
Finite element model; the outside and inside views

a constrained optimization scheme, are provided in the article by Kawa et al. [19]. The resulting values of

$$\Omega_1^{\sigma_0} = 0.21;\ \sigma_{01} = 0.23;\ \sigma_{02} = 0.95;\ \sigma_{03} = 1.55$$
$$\Omega_1^{\varphi} = -0.15;\ \phi_1 = 59.22;\ \phi_2 = -21.40;\ \phi_3 = -676.55$$
$$\Omega_1^{c} = -0.40;\ c_1 = 0.50;\ c_2 = 12.20;\ c_3 = -15.69$$

the best-fit coefficients are:

The superstructure of the Paugan powerhouse is composed of structural steel single bay frames, spaced 7.30 m c/c along the entire length of 146 m of the structure. Unreinforced non-bearing masonry walls, incorporating the columns of the steel frames, serve as enclosures. The height of the walls is 16.5 m; the walls are of variable thickness, from 0.425 m to 1.0 m, and accommodate a series of large window frames. The outside and inside views of the powerhouse are presented in Fig. 4.

The finite element model is shown in Fig. 5 and consists of the concrete slab, concrete and steel columns, the steel frame, the powerhouse roof, and the brick wall with the window openings. The details of the finite element model were as follows:

- total no of elements: 125,137; element types: upstream concrete slab and powerhouse roof – thick shell elements, concrete and steel column – 3D beam elements, brick wall-solid brick elements with homogenized properties, weight above the roof-point mass elements; connection between the frame and the bricks as well as between the column and the bricks – interface contact elements.

The primary dynamic simulations, following the time history of the earthquake, were carried out in two steps, viz. linear and non-linear analysis. Both incorporated self weight combined with deformations at the base caused by a continuing alkali-aggregate reaction. The earthquake record typical for the region of Paugan (maximum ground acceleration of 0.414 g in the horizontal direction and 0.276 g in the vertical direction) was adopted. For the linear elastic

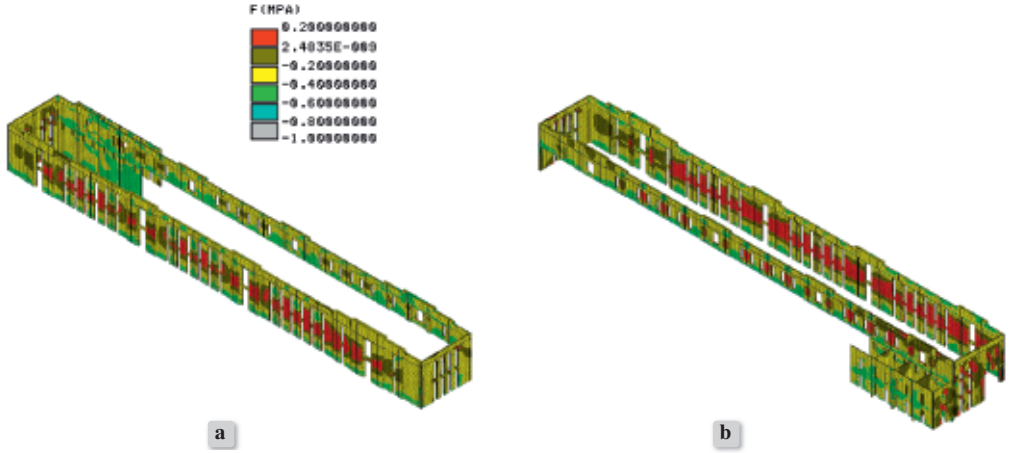

Figure 6.
The distribution of the maximum value of the failure function; (a) the outside and (b) inside views

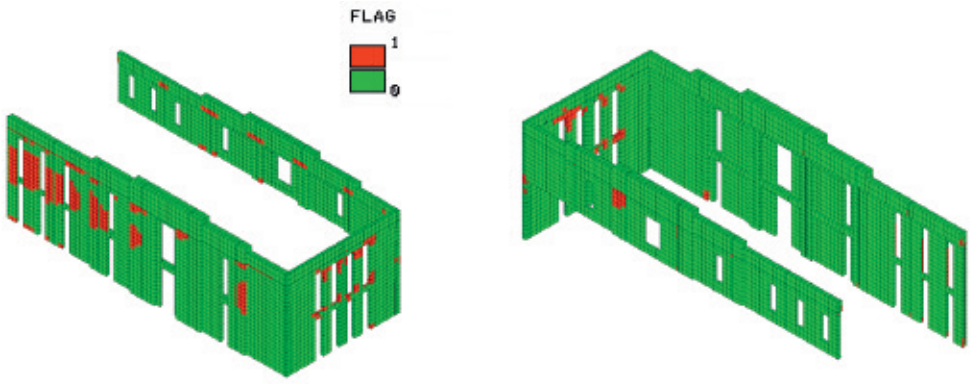

Figure 7.
The cracked regions; flag of zero (0) indicates no cracking; one (1) indicates cracking has occurred

analysis, the plastic admissibility of the stress field (for the time step producing maximum values of failure function) was assessed by invoking the macroscopic failure criterion (5). If the stress field was admissible the analysis was terminated, otherwise a non-linear dynamic analysis was carried out, based on the framework outlined in Section 2.1.2.

The results of the linear dynamic analysis, viz. the evaluation of the admissibility of the stress field, are presented in Fig. 6. The figure shows the distribution of the maximum value of the failure function F, Eq.(5). In general, in the regions experiencing $F>0$ (shown in red) the stress state is plastically inadmissible, i.e. will result in formation of cracks in the brickwork. The contours of the value of F are shown on the outside (a) and inside (b) faces, respectively.

The distribution of F indicates that a linear dynamic analysis is not adequate in this case. The results of non-linear analysis, in terms of distribution of damage zones, are shown in Fig. 7. By examining these results one may conclude that, in spite of local cracking, the walls will sustain the seismic load without the loss of stability. To ensure that large fragments of masonry do not detach from the walls, a light reinforcement is suggested.

The main reinforcement strategy examined here consisted of adding an additional attachment to the steel structure in the regions of potential cracking of the brick panel, using anchor bolts. Fig. 8a shows the positioning of the bolts. A total of 3 bolts per column, having "S" shaped heads, are recommended in the upper portion of the wall. The numerical analysis carried out demonstrated that the bolts would be more effective if their rigidity was properly calibrated. For each bolt the required optimum stiffness was obtained by adding a dumper attaching the anchor to the column.

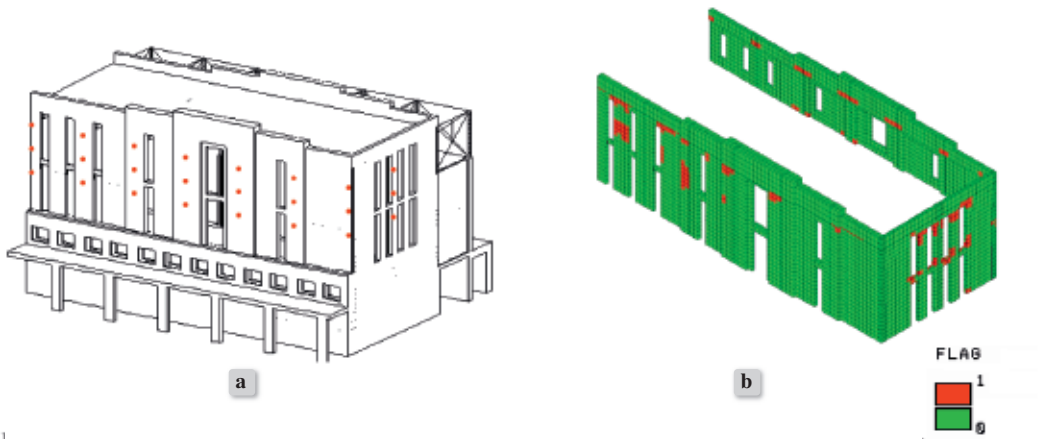

Figure 8.
(a) Location of the reinforcing bolts (marked in red) in downstream wall; (b) cracked regions after reinforcement

The key results of the dynamic analysis for the reinforced walls are provided in Fig. 8(b). A significant improvement in the structural behaviour is evident when comparing these results with those shown in Fig. 7.

3. NUMERICAL ANALYSIS OF LARGE-SCALE REINFORCED CONCRETE STRUCTURES

The other type of structured material considered here is the heavily reinforced concrete. The durability of both concrete and reinforced concrete structures is often significantly impaired by the alkali-aggregate reaction (AAR). The product of the reaction is a gel that forms around the aggregate particles; it imbibes water from the pore fluid and expands triggering a progressive damage of the material. The work outlined here is primarily concerned with application of a non-linear continuum model which was recently developed [13] for the description of mechanical behaviour of reinforced concrete subjected to AAR. The model is an extension of the framework presented earlier [10], in which the reinforced concrete is considered as a composite medium comprising concrete matrix and two orthogonal families of reinforcement. The latter formulation is generalized to incorporate the chemo-mechanical interaction associated with continuing AAR.

In what follows, the governing constitutive relations, which have been incorporated in a finite element code, are first outlined. Later, the results of some recent numerical studies are presented, which involve the analysis of nuclear structures affected by the chemical degradation (cf. Ushaksaraei, Pietruszczak & Gocevski [20]). In particular, the results that pertain to some structural elements within the Gentilly-2 (G2) nuclear powerplant, situated near the community of Trois-Rivières in Quebec, are examined.

3.1. Formulation of the problem

The description of mechanical effects of AAR within the *concrete matrix* incorporates a scalar parameter ζ which is a measure of the continuing reaction and is defined as

$$\zeta(t)=\frac{\epsilon(t)}{\bar{\epsilon}}; \qquad \bar{\epsilon}=\epsilon(t\to\infty) \tag{7}$$

Here, $\epsilon(t)$ is the volumetric expansion of concrete and $\bar{\epsilon}$ is a material parameter that defines the maximum value of ϵ, for a given alkali content, in the stress free state. The evolution law is assumed in a simple linear form

$$\dot{\zeta}=\gamma(\bar{\zeta}-\zeta) \quad \text{for } t\geq t_0 \;\Rightarrow\; \zeta=\bar{\zeta}(1-e^{-\gamma\langle t-t_0\rangle}); \qquad \zeta=0 \quad \text{for } t<t_0 \tag{8}$$

where $\bar{\zeta}$ can be interpreted as a value of the state variable ζ associated with the chemical equilibrium, γ is a material constant describing rate of the reaction, and t_0 is the initiation time. The closed form integration for ζ in Eq. (8) is based on a constant value of $\bar{\zeta}$, where $<\ldots>$ are Macauley brackets. The value of $\bar{\zeta}$ depends, in general, on the confining pressure, temperature and relative humidity.

The formulation of the constitutive relation that governs the chemo-mechanical interaction follows the framework established in an earlier article by Pietruszczak and Gocevski [21]. In the *elastoplastic* range, the additivity of elastic and plastic strain rates

leads to

$$\dot{\boldsymbol{\varepsilon}} = [C^e]\dot{\boldsymbol{\sigma}} + \mathbf{b}\dot{\zeta} + \dot{\boldsymbol{\varepsilon}}^p \quad \Rightarrow \quad \dot{\boldsymbol{\sigma}} = [D^e](\dot{\boldsymbol{\varepsilon}} - \dot{\boldsymbol{\varepsilon}}^p - \mathbf{b}\dot{\zeta}); \qquad (9)$$
$$\mathbf{b} = \frac{\partial}{\partial \zeta}[C^e]\boldsymbol{\sigma} + \frac{1}{3}\bar{\in}\,\boldsymbol{\delta}$$

in which $[D^e]=[C^e]^{-1}$, where $[C^e]$ is the elastic compliance. In order to define the plastic strain rates, the functional form of the yield criterion $f=0$ is assumed to be affected by the progress in the reaction, i.e. $f=f(\boldsymbol{\sigma},\boldsymbol{\varepsilon}^p, \zeta)$. Following a standard plasticity procedure, the constitutive relation can be obtained as

$$\dot{\boldsymbol{\varepsilon}} = [C]\dot{\boldsymbol{\sigma}} + \boldsymbol{\Gamma}\dot{\zeta}; \qquad (10)$$
$$\boldsymbol{\Gamma} = \mathbf{b} + \frac{1}{H}\frac{\partial f}{\partial \zeta}\frac{\partial Q}{\partial \boldsymbol{\sigma}} = \frac{\partial}{\partial \zeta}[C^e]\boldsymbol{\sigma} + \frac{1}{H}\frac{\partial f}{\partial \zeta}\frac{\partial Q}{\partial \boldsymbol{\sigma}} + \frac{1}{3}\bar{\in}\,\boldsymbol{\delta}$$

where

$$[C] = [C^e] + \frac{1}{H}\frac{\partial Q}{\partial \boldsymbol{\sigma}}\left(\frac{\partial f}{\partial \boldsymbol{\sigma}}\right)^T; \quad H = -\left(\frac{\partial f}{\partial \boldsymbol{\varepsilon}^p}\right)^T\frac{\partial Q}{\partial \boldsymbol{\sigma}} \qquad (11)$$

In the equations above, [C] is the elastoplastic compliance operator, H is the plastic hardening modulus and $\boldsymbol{\delta}$ is the Kronecker's delta.

For reinforced concrete, the problem is formulated in two stages [10]. Stage I deals with the homogeneous deformation mode prior to cracking of the concrete matrix, whereas stage II involves a localized deformation associated with formation of macrocracks.

– *Stage I (prior to cracking)*

The problem is referred to the frame of reference x^*, such that x_2^* and x_3^* are along the axes of reinforcement. The average macroscopic stress/strain rates for the composite body are defined through the volume averaging procedure, i.e.

$$\dot{\boldsymbol{\sigma}}^* = \eta_1\dot{\boldsymbol{\sigma}}_1^* + \eta_2\dot{\boldsymbol{\sigma}}_2^* + (1-\eta_1-\eta_2)\dot{\boldsymbol{\sigma}}_m^*;$$
$$\dot{\boldsymbol{\varepsilon}}^* = \eta_1\dot{\boldsymbol{\varepsilon}}_1^* + \eta_2\dot{\boldsymbol{\varepsilon}}_2^* + (1-\eta_1-\eta_2)\dot{\boldsymbol{\varepsilon}}_m^* \qquad (12)$$

where η_1 and η_2 represent the volume fractions of the respective sets of reinforcement, whereas $\dot{\boldsymbol{\sigma}}_k^*$, $\dot{\boldsymbol{\varepsilon}}_k^*$ ($k=1,2,m$)are the averages of stress/strain rates in the constituents involved. Both these local fields are assumed to be homogeneous within themselves, so that

$$\dot{\boldsymbol{\varepsilon}}_1^* = [C_1^*]\dot{\boldsymbol{\sigma}}_1^*; \quad \dot{\boldsymbol{\varepsilon}}_2^* = [C_2^*]\dot{\boldsymbol{\sigma}}_2^*; \quad \dot{\boldsymbol{\varepsilon}}_m^* = [C_m^*]\dot{\boldsymbol{\sigma}}_m^* + \boldsymbol{\Gamma}^*\dot{\zeta} \qquad (13)$$

where $[C^*]$'s are the compliance operators. The reinforcing steel is considered to be an elastic-perfectly plastic von Mises material obeying an associated flow rule, while the behaviour of concrete matrix is governed by eq.(10).

The local stress rate averages can be related to the overall macroscopic measure $\dot{\boldsymbol{\sigma}}^*$ viz.

$$\dot{\boldsymbol{\sigma}}_1^* = [B_1]\dot{\boldsymbol{\sigma}}^* + [\bar{B}_1]\boldsymbol{\Gamma}^*\dot{\zeta};$$
$$\dot{\boldsymbol{\sigma}}_2^* = [B_2]\dot{\boldsymbol{\sigma}}^* + [\bar{B}_2]\boldsymbol{\Gamma}^*\dot{\zeta}; \qquad (14)$$
$$\dot{\boldsymbol{\sigma}}_m^* = [B_m]\dot{\boldsymbol{\sigma}}^* + [\bar{B}_m]\boldsymbol{\Gamma}^*\dot{\zeta}$$

The details on the specification of operators [B] and [$\bar{B}$], based on imposing some explicit kinematic constraints, are provided in the original reference.

Combining the above equations, the macroscopic constitutive relation can be established

$$\dot{\boldsymbol{\varepsilon}}^* = [C^*]\dot{\boldsymbol{\sigma}}^* + [\bar{C}^*]\boldsymbol{\Gamma}^*\dot{\zeta}; \qquad (15)$$
$$[C^*] = \{\eta_1[C_1^*][B_1] + \eta_2[C_2^*][B_2] + (1-\eta_1-\eta_2)[C_m^*][B_m]\};$$
$$[\bar{C}^*] = \{\eta_1[C_1^*][\bar{B}_1] + \eta_2[C_2^*][\bar{B}_2] + (1-\eta_1-\eta_2)([C_m^*][\bar{B}_m] + [I])\}$$

Apparently, the macroscopic stress/strain rates can be transformed to an arbitrarily chosen global Cartesian system by following the standard transformation rules.

The above equation defines the response of the composite prior to formation of macrocracks in the concrete matrix. In reinforced concrete structures, the cracking is typically associated with the tensile stress regime. Once a macrocrack forms, the formulation of the problem follows the procedure that is conceptually similar to that outlined in Section 2.1, viz. eqs. (4)-(5).

– *Stage II (after formation of a macrocrack)*

The representative volume of the material comprises now the "intact" reinforced concrete intercepted by a macrocrack of a given orientation $\boldsymbol{n}$. The latter represents a composite medium within itself as it consists of a zone of fractured concrete reinforced with steel bars.

The procedure incorporates the stress/strain rate averaging and the deformation within the fractured zone (f) is defined in terms of velocity discontinuities across the interface, $\dot{g}_i$. The constitutive relations governing the behaviour of the intact material (i) and the interface are expressed as

$$\dot{\boldsymbol{\varepsilon}}_i = [C]\dot{\boldsymbol{\sigma}}_i + [\bar{C}]\boldsymbol{\Gamma}\dot{\zeta};$$
$$\dot{\boldsymbol{\varepsilon}}_f = \frac{1}{h}[N]\dot{\boldsymbol{g}}; \qquad \dot{\boldsymbol{g}} = [K]^{-1}\dot{\boldsymbol{t}}; \qquad \dot{\boldsymbol{t}} = [N]^T\dot{\boldsymbol{\sigma}}_i \qquad (16)$$

where [K] denotes the stiffness of the fractured zone, $\boldsymbol{t}$ is the traction vector, and h denotes the thickness of the cracked zone. The averaged macroscopic constitutive relation is defined by imposing the continuity of traction along the interface, which leads to

$$\dot{\boldsymbol{\varepsilon}} \simeq ([C]+\mu[N][K]^{-1}[N]^{T})\dot{\boldsymbol{\sigma}} + [\bar{C}]\boldsymbol{\Gamma}\dot{\zeta} \tag{17}$$

Here, $\mu = \mu_f / h$ represents the ratio of the area of the fractured zone to the representative volume of the sample. Thus μ is, in fact, independent of h.

The approach outlined above requires an assessment of the mechanical properties of the fractured zone, viz. operator [K]. This zone is composed of the damaged concrete and the network of reinforcement. The details on the description of mechanical characteristics are provided in the article by Pietruszczak & Winnicki [10].

The particular formulation employed here to describe the nonlinear behaviour of concrete matrix is similar to that outlined by Pietruszczak et al. [22]. It invokes a non-associated flow rule and the yield surface is expressed in a functional form

$$f = \bar{\sigma} - \alpha(\zeta)\,\beta(\xi)\,k(\theta)\,\bar{\sigma}_c = 0; \quad \xi \propto (\frac{1}{2}\dot{e}^p_{ij}\dot{e}^p_{ij})^{1/2};$$
$$\bar{\sigma}_c = \frac{-a_1 + \sqrt{a_1^2 + 4a_2\,(a_3 + I/f_c)}}{2a_2}\, f_c \tag{18}$$

In the equations above, σ_m, $\bar{\sigma}$ and θ represent again a set of invariant measures of the stress tensor [15], while a's are material constants normalized with respect to axial compressive strength (f_c); The degradation of strength properties is governed here by the variable $\alpha(\zeta)$. In general, all degradation functions, for elastic moduli as well as strength, are assumed in a simple linear form

$$E = E_0\,[1-(1-B_1)\zeta];$$
$$\nu = \nu_0\,[1-(1-B_2)\zeta]; \tag{19}$$
$$\alpha = 1-(1-B_3)\zeta$$

where B's are material parameters. Finally, in the simulations presented here, the parameter $\bar{\zeta}$ has been taken as a function of the confining pressure (for a fixed value of temperature and humidity), and its evolution has been described via an exponential form

$$\bar{\zeta} = e^{-A_1\sqrt{\frac{\langle -tr(\boldsymbol{\sigma})\rangle}{3f_c}}} \tag{20}$$

where A_1 is a material constant.

3.2. Numerical analysis; simulations of structural elements of a nuclear power plant

In this part, the mathematical framework described in Section 3.1 is illustrated by some numerical examples that involve selected structural elements within the G2 nuclear powerplant. In particular, the simulations presented here pertain to the containment structure, the fuel exchange room R2-001 in the reactor building as well as the spent fuel storage pool. The analysis involves modeling of continuing AAR as well as the non-linear simulation of a seismic event using earthquake characteristics typical for G2 site.

– *Containment structure*

The evolution of damage within the concrete walls of the containment structure of G2 is examined first. The main issue, after 27 years of operation, is the ultimate pressure capacity (UPC) and the air tightness of the reinforced concrete envelope. The discretized structure is shown in Fig. 9. The basic properties of concrete and reinforcement were:

Concrete: E = 34.5 GPa; ν = 0.2; f_{co} = 35 MPa; f_{to} = 2.2 MPa

Reinforcement: E = 200 GPa; ν = 0.3; σ_Y = 400 MPa

while the values of parameters governing the kinetics of AAR were taken as $\bar{\varepsilon}$ = 0.0104 ; γ = 0.0104 (1/day); B_1=0; B_2=0; B_3=0.9; A_1=8.3

The perimeter wall has circumferential and vertical post-tensioning tendons while the upper dome consists of three layers of superimposed tendons. The equivalent initial compressive stresses in the concrete sections were evaluated based on spacing of the cables. The average values range from 10.7 MPa (for both components in spherical plane of the superior dome) to 5.9 MPa for circumferential and 3.5 MPa for vertical direction of the wall. In addition, the structure is heavily reinforced with two families of steel bars.

The key results describing the response of the structure under own weight, post-tensioning, and the ongoing AAR are shown in Fig. 10. The reaction had

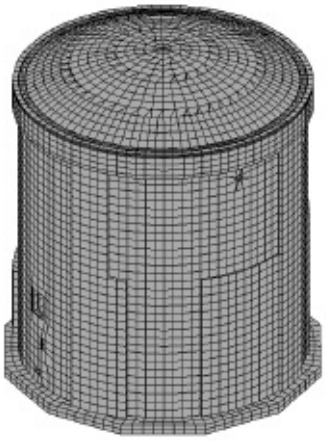

Figure 9.
Discretazation of the containment structure

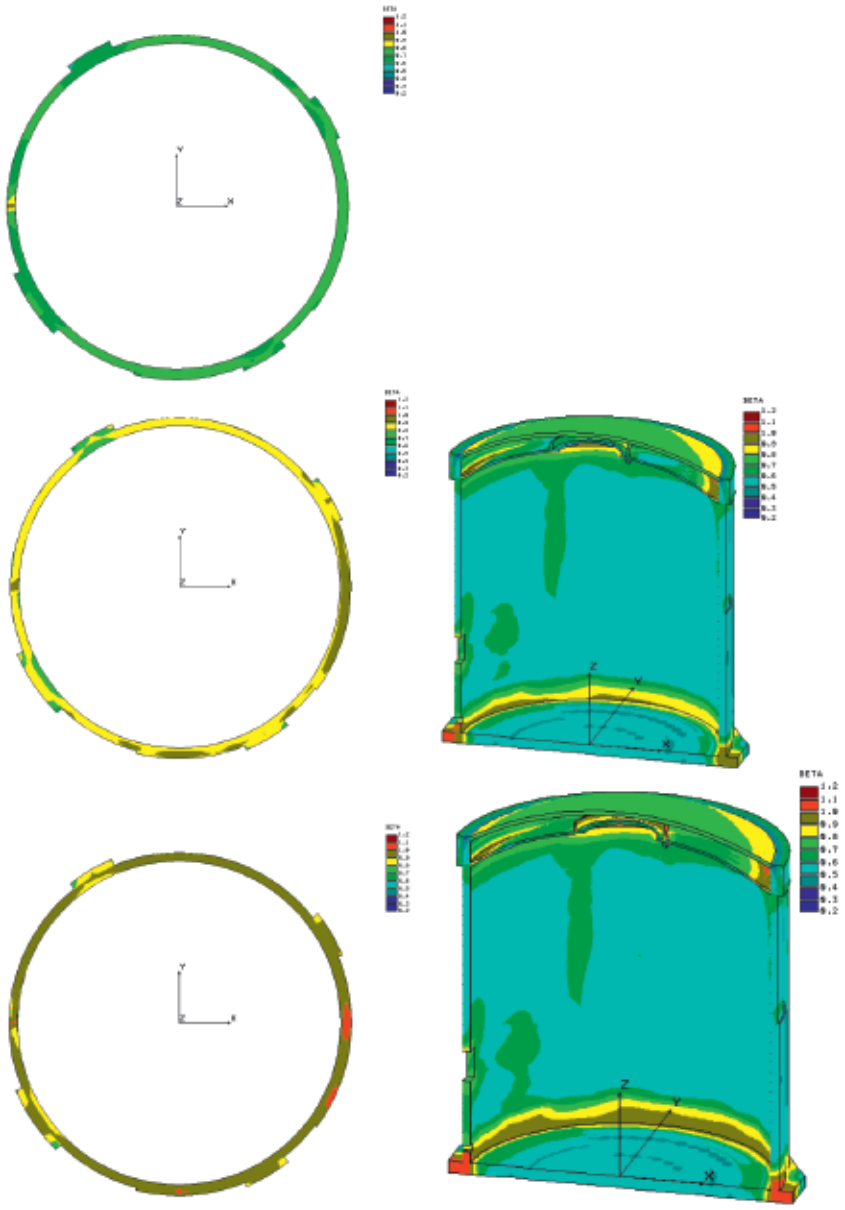

Figure 10.
Distribution of damage factor, β , due to work load and the AAR continuing for 12 years (onset of micro-cracking), 17 years, and 32 years from top to bottom, respectively); horizontal section at z = 1.41 m

started around 1985 and has been continuing since. The figure presents the distribution of damage factor, β, eq.(18), after 12, 17, and 32 years of the reaction. Note that the values of β >1 (shown in red) are indicative of an unstable response associated with formation of macrocracks. The results point to the presence of a damage zone, which at some locations penetrates through the thickness of the wall. However, the macrocracks are not more than 0.15 mm wide. In general, the extent of damage after over 30 years of continuing AAR is not very significant. The containment is structurally sound and only minor refurbishment from inside the building may be required to ensure adequate air tightness.

The air tightness is also examined in Fig. 11, which shows the simulation of internal pressure test (125 kPa). The figure presents the distribution of damage following the pressure test. The intensity of damage is highest in the upper part of the wall, close to the dome, where the value β reaches 0.9. The latter is indicative of formation of microcracks. Indeed the test showed that there is a minor air loss at exactly the

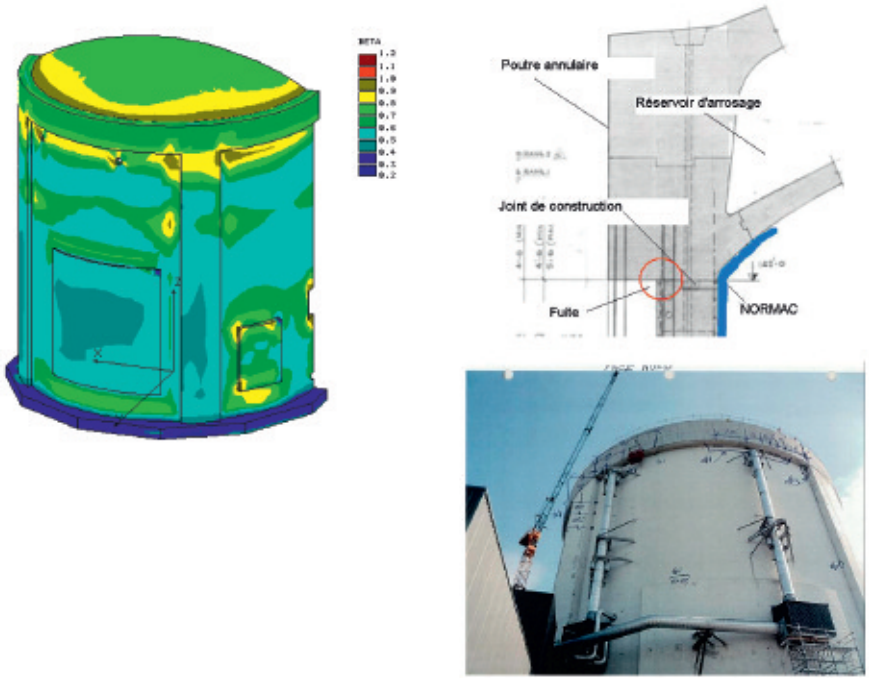

Figure 11.
Distribution of damage factor, β, following an internal pressure test (125 MPa)

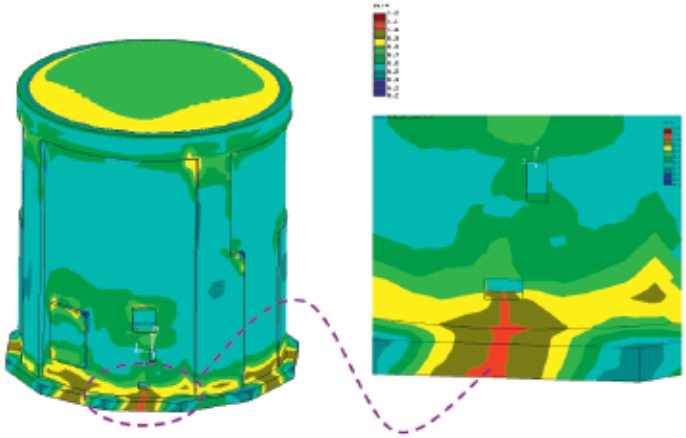

Figure 12.
Distribution of damage factor, β, following an earthquake after 30 years of continuing reaction

same location that is triggered by the presence of microcracks visible inside the structure.

Finally, the response of the structure under a seismic excitation, typical for G2 site, has been examined. Fig.12 shows the extent of damage that corresponds to 30 years of continuing reaction (year 2015) following an earthquake. It is evident that vertical macrocracks (shown in red) now form in the region directly under the opening.

– Fuel exchange room and the spent fuel pool in the nuclear reactor building

The geometry and FE discretization for the fuel exchange room R-0021 is shown in Fig. 13. The AAR-affected parts, with different ultimate free expansions, are detailed in the adjacent figure. The remaining part of the structure is assumed to consist of reinforced concrete exhibiting an elastic behaviour. The same figure shows the superimposed distribution of the damage factor β after 30 years of AAR. The cracked regions, i.e. those with $\beta > 1$, are again marked in dark

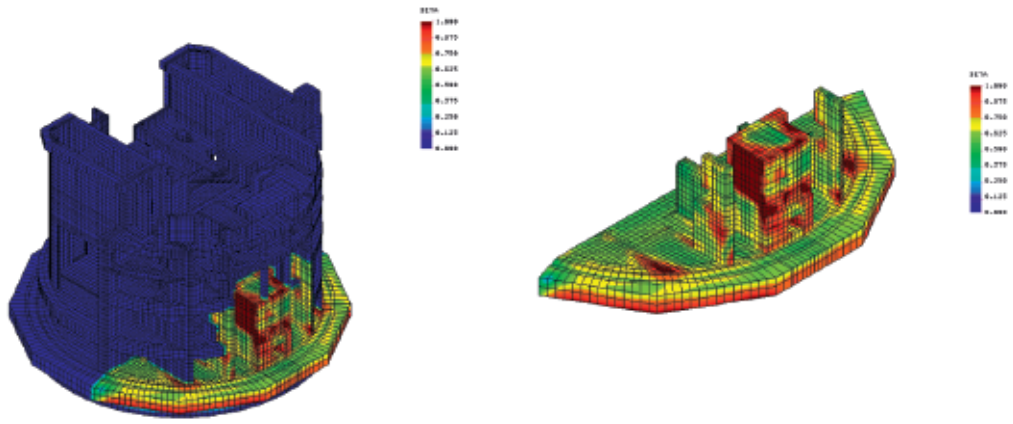

Figure 13.
FE discretization and distribution of damage factor, β, after 30 years of AAR, in the interior of G2: entire structure (left); AAR-affected parts (right)

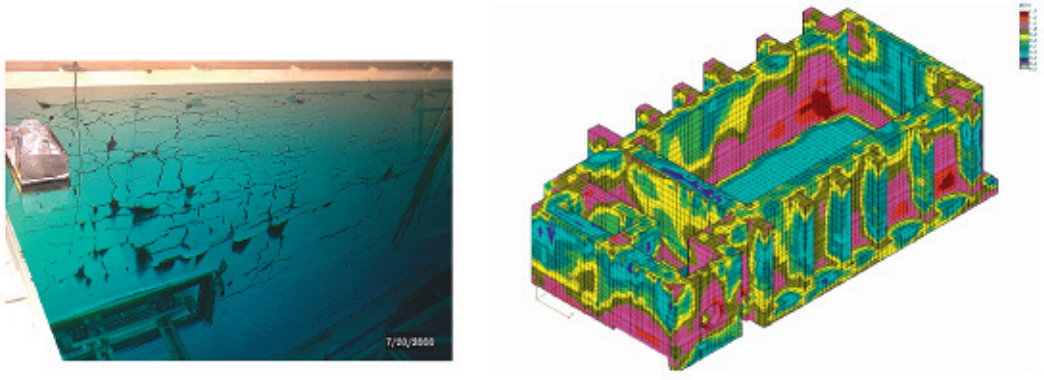

Figure 14.
Spent fuel storage pool; cracking after 30 years as a result of continuing AAR

red. It is evident here that the damaged zones appear on the wall surfaces, where the expansion of concrete due to AAR is high. The cracking through the wall cross-sections is not very significant however. In general, additional studies combined with in-situ tests are required for a better calibration of the numerical model in order to assess whether the local cracking has an effect on air tightness of the concrete. The concrete aging management program presently under preparation will insure that adequate repairs are undertaken, if needed, so that the plant safety is never compromised.

Finally, Fig. 14 deals with extent of cracking in the spent fuel storage pool as a result of continuing AAR. The figure shows again the distribution of the damage factor after 30 years of the reaction. It is evident that inside the pool there are regions where the macrocracks form. Those cracks are clearly visible inside the structure, as evidenced in the photograph that is attached.

4. FINAL REMARKS

The work reported here presents the strategies for analysing large-scale masonry and heavily reinforced concrete structures. This study clearly demonstrates that, given the complex geometry, a conventional approach, based on simplistic standards/guidelines adopted by consulting engineering offices, would not be adequate here. In all cases, an appropriate non-linear finite element analysis is required, examining the history of loading, to asses the extent of damage and the efficiency of the proposed refurbishing strategies.

For masonry structures, the suggested methodology is to employ a homogenization procedure to generate the data on the directional dependence of the mechanical response based on properties of constituents. Given this data, the macroscopic material functions appearing in the continuum formulation can then be identified. Note that in this approach the only experimental information required is that on

isotropic strength/deformation properties of constituents, which can be obtained from standard material tests.

For heavily reinforced large-scale concrete structures, the presence of reinforcement cannot be modeled in a discrete sense. Thus, the reinforced concrete should also be considered as a composite medium comprising the concrete matrix and a set of families of reinforcement. The overall macroscopic behaviour can then be defined by employing suitable averaging techniques and the chemo-mechanical interaction can be accounted for by incorporating the framework of chemo-plasticity.

ACKNOWLEDGEMENT

The large-scale simulations presented here have been conducted with collaboration and financial support from Hydro-Quebec, Montreal. A significant contribution of Dr. R. Ushaksaraei (McMaster University) and Dr. V. Gocevski (Hydro-Quebec) is acknowledged.

This paper was presented at the 7th Intern. Conf. on Analytical Models and New Concepts in Concrete and Masonry Structures (AMCM'2011), Krakow, June 2011.

REFERENCES

[1] *Sulem J., Muhlhaus H.B*; A continuum model for periodic two-dimensional block structures. Mech. Coh. Frict. Mater., Vol.2, 1997; p.31-46

[2] *Masiani, R., Trovalusci, P.*; Cauchy and Cosserat materials as continuum models of brick masonry. Meccanica, Vol.31, 1996; p.421-432

[3] *Anthoine, A.*; Derivation of in-plane elastic characteristics of masonry through homogenization theory. Int. J. Solids Struct., Vol.32, 1995; p.137-163

[4] *Anthoine, A.*; Homogenization of periodic masonry: plane stress, generalized plane strain or 3D modelling? Commun. Numer. Meth. Eng., Vol.13, 1997; p.319-326

[5] *Lourenço, P.B., Rots, J.G., Blaauwendraad, J.*; Continuum model for masonry: parameter estimation and validation. J. Struct. Eng., ASCE, Vol.124, No.6, 1998; p.642-652

[6] *Raffard, D., Duveau, G., Shao, J.F. Henry, J.P.*; Numerical homogenization of a masonry volume. In: Computer methods in structural masonry – 5, Computers & Geotechnics Ltd., Swansea, 2001; p.43-51

[7] *Ushaksaraei, R. Pietruszczak, S.*; Failure criterion for structural masonry based on critical plane approach. J. Eng. Mech. ASCE, Vol.128, 2002; p.769-778

[8] *Scordelis, A. C.*; Finite element analysis of reinforced concrete structures (survey paper). Proc., Spec. Conf. on the FEM in Civil Eng., Montreal, 1972; p.71-113

[9] *Crisfield, M. A., Wills, J.*; Analysis of RC panels using different concrete models. J. Eng. Mech., Vol.115, 1989; p.578-597

[10] *Pietruszczak, S., Winnicki, A.*; Constitutive model for concrete with embedded sets of reinforcement. J. Eng. Mech., ASCE, Vol.129, 2003; p.725-738

[11] *Page, A.W.*; The biaxial compressive strength of brick masonry. Proc. Inst.Civil Engrs., Vol.71, 1981; p.893-906

[12] *Page, A.W.*; The strength of brick masonry under biaxial tension-compression. Int. J. Masonry Constr., Vol.3, 1983; p.26-31

[13] *Winnicki, A., Pietruszczak, S.*; On mechanical degradation of reinforced concrete affected by alkali-silica reaction. J. Eng. Mech., ASCE, Vol.134, 2008; p.611-627

[14] *Shieh-Beygi, B., Pietruszczak, S.*; Numerical analysis of structural masonry: mesoscale approach. Int.J.Comp.Struct., Vol.86, 2008; p.1958-1973

[15] *Nayak, G.C., Zienkiewicz, O.C.*; Elastoplastic stress analysis. Generalization of various constitutive equations including stress softening. Int. J. Num. Meth. Engng., Vol.5, 1972; p.113-135

[16] *Pietruszczak, S.*; On homogeneous and localized deformation in water-infiltrated soils. Int. J. Damage Mech., Vol.8, 1999; p.233-253

[17] *Pietruszczak S., Mróz Z.*; On failure criteria for anisotropic cohesive-frictional materials. Intern. Journ. Num. Anal. Meth. Geomech., Vol.25, 2001; p.509-524

[18] *Pietruszczak S., Gocevski V.*; Seismic analysis of brick masonry structures of the Paugan powerhouse. In: Computational Geomechanics – COMGEO I, ICCE Publ., Rhodes, 2009; p.851-863

[19] *Kawa M., Pietruszczak S., Shieh-Beygi B.*; Limit states for bricks masonry based on homogenization approach. Intern. Journ. Solids & Structures, Vol.45, 2008; p.998-1016

[20] *Ushaksaraei R., Pietruszczak S., Gocevski V.*; Seismic analysis of nuclear structures affected by chemical degradation. In: Computational Geomechanics – COMGEO II, ICCE Publ., Rhodes, 2011; p.858-869

[21] *Pietruszczak, S., Gocevski, V.*; On rehabilitation of concrete structures affected by alkali-silica reaction. Int. J. Comp. Civil & Struct. Eng., Vol.1, No.3, 2002; p.182-197

[22] *Pietruszczak, S., Jiang, J., Mirza, F.A.*; An elastoplastic constitutive model for concrete. Int. J. Solids Struct., Vol.24, 1998; p.70-722